Old Dominion University
ODU Digital Commons

Mechanical & Aerospace Engineering Faculty Publications | Mechanical & Aerospace Engineering

2024

Fabrication of Smooth SAC305 Thin Film Via Magnetron Sputtering

M. Ojha
Old Dominion University

A. A. Elmustafa
Old Dominion University

Follow this and additional works at: https://digitalcommons.odu.edu/mae_fac_pubs

Part of the Electrical and Electronics Commons, Electro-Mechanical Systems Commons, and the Semiconductor and Optical Materials Commons

Original Publication Citation

Ojha, M., & Elmustafa, A. A. (2024). Fabrication of smooth SAC305 thin film via magnetron sputtering. *Journal of Materials Science: Materials in Electronics*, *35*(16), 1-16, Article 1100. https://doi.org/10.1007/s10854-024-12799-8

This Article is brought to you for free and open access by the Mechanical & Aerospace Engineering at ODU Digital Commons. It has been accepted for inclusion in Mechanical & Aerospace Engineering Faculty Publications by an authorized administrator of ODU Digital Commons. For more information, please contact digitalcommons@odu.edu.

J Mater Sci: Mater Electron **(2024) 35:1100**

Fabrication of smooth SAC305 thin film via magnetron sputtering

M. Ojha[1] and A. A. Elmustafa[1,*]

[1] *Department of Mechanical and Aerospace Engineering and The Applied Research Center-Thomas Jefferson National Accelerator Facility, Old Dominion University, Norfolk, VA, USA*

Received: 24 March 2024
Accepted: 16 May 2024
Published online:
8 June 2024

© The Author(s), 2024

ABSTRACT

SAC305 (96.5 wt% Sn, 3 wt% Ag, 0.5 wt%Cu) solder is increasingly becoming popular due to its reliability good characteristics and performance in addition to the environmental concerns and regulations that restrict the use of lead in nano/microelectronic products. In nano/microelectronics, manufacturing smooth solder coatings free of defects such as voids and cracks, which can compromise joint reliability is crucial. Magnetron sputtering offers a high degree of control over film thickness and composition, resulting in films with excellent uniformity and adhesion. Despite these advantages, fabricating continuous and robust SAC305 films using magnetron sputtering remains a difficult task with limited research addressing these Challenges. To address these challenges and obtain an enhanced surface morphology property, we focus on fabricating SAC305 thin films by optimizing the magnetron sputtering parameters including sputtering power and pressure, and by using various substrates. Field emission-scanning electron microscopy imaging, energy-dispersive X-ray spectroscopy, X-ray diffraction, and atomic force microscopy were used to evaluate the quality of the thin films.

1 Introduction

Electronic devices consist of various components, including resistors, transistors, capacitors, inductors, diodes, and others. These components are interconnected using solders at various levels to ensure mechanical and electrical continuity. The interconnection technology has advanced from conventional automated wire and tape bonding to flip-chip technology due to reliability, high electrical performance, and package miniaturization [1, 2]. Sn–Pb solder alloys have been widely used in nano/microelectronics due to their low melting temperature and good wetting properties, but they are being phased out due to regulations and Pb toxicity concerns [3]. SAC305 (96.5%Sn–3%Ag–0.5%Cu) solder is evolving as a promising alternative material to Sn–Pb solders due to its low eutectic temperature, exceptional conformity with other components, non-toxicity, and superb mechanical/structural properties [4–6].

The rapid evolution of digital electronics, exemplified by Artificial Intelligence (AI) and high-performance computing (HPC), has created unprecedented demands for computers with remarkable memory,

Address correspondence to E-mail: aelmustafa@odu.edu

https://doi.org/10.1007/s10854-024-12799-8

speed, and computational capabilities. In response to these demands, the number of transistors per unit area on microchips has been exponentially increasing, in line with Moore's Law, while chip sizes continue to shrink. However, to address the growing complexity of system integration requirements, such as high I/O connections, there is a critical need for the development of smooth and continuous thin film solders. Such solders must facilitate fast signal transfer, minimize power consumption, and efficiently dissipate heat. Achieving a smooth and continuous surface topography in the deposited solder is essential for its effective use in nano/microelectronics applications. Additionally, the microstructure and properties of the solder joints significantly influence their performance. Specifically, thin film solders with smooth surfaces and without imperfections yield superior electrical and thermal conductivity, strong adhesion, and exceptional reliability [7–10]. The microstructural characteristics of these micro and nanoscale solders are not fully understood. Further research could lead to the optimization of the joining processes and improve the electrical properties and reliability of the joints through the establishment of correlations between fabrication, microstructure, and properties.

In general, the properties of deposited thin films depend on numerous factors, such as substrate type, substrate cleaning, pressure, gas type, gas flow, temperature, current density, and bias voltage [11]. However, adjusting these parameters could impact films' deposition rate, adhesion, grain size, and thickness resulting in different film morphology, microstructure, hardness, Young's modulus, and electrical resistivity [12]. Magnetron sputtering is one of the traditional methods for depositing solder alloys onto chip bond pads in flip-chip technology. In magnetron sputtering, materials are transported atom by atom in a vacuum chamber from a target and deposited onto a substrate surface [13]. The film thus produced has various advantages over films produced by other PVD methods, such as excellent mechanical properties, good adhesion to the substrate, high deposition rate, good thickens uniformity, and scalability to large areas [14, 15]. Chan and Teo [16] demonstrated that controlling sputtering power and deposition pressure in DC magnetron sputtering of copper films on p-type Si led to optimized growth, improved deposition rates, excellent electrical properties, and structural quality. Similarly, Shah et al. (2010) stated that working pressure, temperature, and power significantly affected the microstructural characteristics of Chromium Nitride (CrN) films deposited on Si(100) substrates using reactive magnetron sputtering. The preferred orientation, grain size, crystallinity, and texture coefficient of CrN films depended on the sputtering conditions [17]. However, the fabrication of smooth, continuous, and robust thin SAC305 films is particularly challenging, and limited research has addressed the challenges of fabricating such films. The post-annealing process after deposition is likely to contribute to the improvement of the surface morphology and crystallinity of the thin films. The annealing process for metals consists of three main stages: recovery, recrystallization, and grain growth. In the recovery stage, the metal's physical properties, such as thermal expansion and electrical conductivity, are restored as dislocations in the crystal move to stress-free environments [18, 19]. This process softens the metal and sets the stage for recrystallization [18, 19]. The metal is heated above its recrystallization temperature during recrystallization, allowing new stress-free grains to replace the deformed ones. The final stage and grain growth occur if annealing continues after recrystallization. This grain growth tends to make the metal's microstructure coarse and hence reduces its strength [18, 19]. Abbas et al. explored the effects of annealing on silver thin films fabricated using physical vapor deposition [20]. The films were annealed at 100 °C to 800 °C in a vacuum oven for 20 min. The study found that lower annealing temperatures resulted in porous, interconnected nanoparticles, while higher temperatures led to distinct nanoparticles of various sizes and shapes [20]. Liu et al. studied the deposition of $Co_{40}Fe_{40}B_{10}Dy_{10}$ thin films on glass substrates using DC magnetron sputtering [21]. The films, with 10 to 50 nm thicknesses, were heat-treated at temperatures between 100 and 300 °C. A notable outcome, the surface roughness (R_a) decreased as the annealing temperature increased, suggesting that higher annealing temperatures produce smoother films [21].

To produce continuous and robust SAC305 thin films represented a mounting challenge that required optimizing the magnetron sputtering parameters including sputtering power and pressure in addition to using various substrates (silicon, gallium arsenide, sapphire, and glass). The goal is to produce SAC305 thin films of enhanced surface morphology properties. Silicon, gallium arsenide, and sapphire are used in the semiconductor industry for various applications [22]. Silicon is the most used semiconductor material

because it is abundant, easy to process, and possesses good electrical properties [22]. Most of the integrated circuits which are the building blocks for electronic devices and solar cells are fabricated from silicon [22]. Gallium arsenide is a compound semiconductor with higher electron mobility and a wider bandgap compared to silicon, making it best suited for high-frequency and high-power applications. Gallium arsenide is used in microwave, radiofrequency, and optoelectronic devices [23]. Sapphire, a crystalline form of aluminum oxide (Al_2O_3) is used as a semiconductor material [24]. Sapphire has a high thermal conductivity and is transparent in the visible and infrared regions, which makes it useful in high-temperature applications and optoelectronics [24]. A comprehensive heat treatment was conducted in a vacuum furnace to improve the surface morphology of the films. The SAC305 thin films were characterized using field emission—scanning electron microscopy (FE-SEM), energy-dispersive X-ray spectroscopy (EDS), and atomic force microscope (AFM).

Ojha et al. [25] discussed SAC305 solder thin film's structural/mechanical properties including creep properties and electrical resistivity measurements. In the current manuscript, we only discuss the process of fabricating SAC305 solder films using various RF and DC sputtering process parameters including pressure and power to fabricate continuous and robust SAC305 films. We also discuss an extensive annealing process that was intended to improve the surface morphology of the fabricated SAC305 films. Additionally, we also present multiple SAC305 films deposited on various substrates (Si, GaAs, sapphire, and glass) and investigate the substrate effect on the quality of the films.

2 Experimental setup

This study investigated the deposition of SAC305 thin films on various substrates: silicon (Si), gallium arsenide (GaAs), sapphire (Al_2O_3), and silicon dioxide (SiO_2). A single high-purity (99.99%) SAC305 (96.5 wt% Sn, 3.0 wt% Ag, 0.5 wt% Cu) 2″ diameter and 0.25″ thick target was acquired from ACI Alloys for all films' depositions. Before deposition, 100 mm diameter substrates of Si, GaAs, Al_2O_3, and SiO_2 were obtained from University Wafers. The Si and GaAs wafers had a thickness of 500 μm and a (100) crystallographic orientation. The Al_2O_3 substrate has a thickness of 650 μm, while the SiO_2 substrate has the same thickness (500 μm) as the Si and GaAs wafers. All substrates were then sectioned into a 2 × 2 cm squares for the deposition process.

The purpose of selecting various substrates is to examine whether the failure of fabricating continuous and robust films is caused by the substrate type. All the Si wafers were prepared by the industry-standard RCA cleaning procedure [26]. The cleaning procedure consists of two stages: standard cleaning-1 (SC-1) and standard cleaning-2 (SC-2). For the SC-1, the Si wafer was dipped into a mixture of water (H_2O), ammonium hydroxide (NH_4OH), and hydrogen peroxide (H_2O_2) with ratios of 5:1:1 for 10 min at 80 °C. This step removes any organic contaminants, oxides, and quartz surfaces from the surface of the substrate wafer. Immediately after that, the wafer was cleaned in deionized (DI) water at room temperature. In the SC-2 stage, the wafer is dipped into a solution of H_2O, hydrochloric acid (HCl), and H_2O_2 with ratios of 5:1:1 for 10 min at 80 °C. This step is envisioned to remove alkali residues and traces of metals, such as Au and Ag, from the wafer surface. The Si wafer was then again cleaned in DI water at room temperature. The Si wafer was exposed to ultrasonic cleaning in an acetone solution for 3 min to eliminate any remaining organic components and residues. A high-pressure nitrogen blower was employed to dry the Si substrate.

An ATC Orion-8 Magnetron Sputter Coater from AJA International was used to sputter the SAC305 films. The chamber features 8 2-in magnetron sputter guns with mechanically controlled shutters operated by pressurized air. A high-performance turbomolecular pump, which is assembled with the system, is intended to reduce the chamber's internal pressure to approximately 1.33×10^{-6} Pa. A gate valve that is connected to the turbomolecular pump regulates this pressure during deposition. The substrate holder is positioned at the top of the chamber, maintaining a distance of 150 mm from the sputter targets. The substrate holder is designed with precise control and versatility. It offers a rotational speed range of 0–40 RPM, to allow for an accurate substrate rotation, and ensure an even, and uniform sputtered coatings. Additionally, the holder features a heating function that can reach up to 850 °C, operable in both local and remote modes. A slow temperature ramp-up is required to prevent warping of the transferable substrate carrier, with a recommended ramp time of 90 min to maximum temperature. Argon gas is the sputtering medium, with its flow rate managed by a mass flow controller. The

chamber is outfitted with three 750 W DC and one 300 W RF sputter gun for versatile sputtering options.

After loading the clean Si wafers to the substrate holder of the RF magnetron sputtering system, the chamber was pumped down to a high vacuum pressure of 5.33×10^{-5} Pa to 1.078×10^{-4} Pa. The Ar flow was kept constant at 20.5 SCCM during deposition. Uniform thickness was accomplished (± 5% error) with a 20 RPM substrate holder rotation, fixed at 150 mm from the target. The base pressure in the chamber before sputtering was 4 Pa. SAC305 thin films were fabricated using DC magnetron sputtering at 200 W power and 0.533 Pa pressure. The deposition was conducted at various temperatures, 24, 50, and 100 °C.

An extensive heat treatment procedure was performed on the sample deposited at room temperature in a vacuum furnace to examine the surface morphology of the thin films. The annealing procedure included changing temperatures from 50 to 220 °C for 1 to 3 h. The process included gradually increasing the temperature at a rate of 12 °C per min. Once the annealing experiment was completed, the sample was kept inside the vacuum chamber until the temperature dropped down to 50 °C. The details of the experiment are summarized in Table 1.

This study investigated the influence of deposition parameters including deposition power and deposition pressure on SAC305 thin films fabricated using RF and DC magnetron sputtering on silicon (Si) substrates at room temperature. The details of the experiment are summarized in Table 2. The minimum possible pressure within the chamber was 0.32 Pa. At this pressure, a minimum power of 20 watts was required to sustain the plasma. The power was varied from 20 to 200 watts while maintaining a constant pressure of 0.4 Pa. Additionally, the pressure was varied from 0.32 to 2.67 Pa while holding the power constant at 200 watts. Exceeding a power of 200 watts at the lowest pressure (0.32 Pa) posed a risk of target burning due to bombardment by high-kinetic-energy argon ions.

Surface morphology analysis of the deposited SAC305 films was performed using JEOL Hitachi S-4700 Field Emission-Scanning Electron Microscopy (FE-SEM). The FE-SEM has a magnification range between ×30 and ×500,000 with spatial resolution of

Table 1 Annealing process of SAC305 thin film at various temperatures

Sample #	Temperature (°C)	Time (h)
1–2	120	1,3
3–4	150	1,3
5–6	180	1,3
7–8	200	1,3
9–10	210	1,3
11	220	1

Table 2 Deposition of SAC305 thin film at various pressures and power

Sample#	DC power (watt)	RF power (watt)	Pressure (Pa)	Time (min)	Deposition Rate (Å/s)	Thickness (μm)
1	20	–	0.4	120	0.35	0.25
2	80	–	0.4	120	1.45	1.04
3	140	–	0.4	120	2.7	1.94
4	200	–	0.4	120	3.9	2.80
5	–	20	0.4	120	0.33	0.24
6	–	80	0.4	120	1.31	0.94
7	–	140	0.4	120	2.16	1.56
8	–	200	0.4	120	2.95	2.08
9	200	–	0.32	120	4	2.88
10	200	–	1.07	120	3.1	2.23
11	200	–	1.87	120	2.24	1.61
12	200	–	2.67	120	1.63	1.17
13	–	200	0.32	120	3.0	2.16
14	–	200	1.07	120	2.3	1.65
15	–	200	1.87	120	1.7	1.22
16	–	200	2.67	120	1.42	1.0

up to 1.5 nm at 15 kV, 12 mm WD and 2.5 nm at 1 k, 2.5 mm WD. Subsequently, the films were mechanically polished with a multi-prep system from Allied High Tech Products Inc., employing high-density, non-woven, low-nap porous cloths. To achieve an ultra-fine surface finish, a 1:3 mixture of abrasive colloidal silica (SiO_2) suspension (0.02 μm diameter) and red lube was used during the polishing process. The polishing which was conducted at a minimal load of 100 g for 2 min, removed approximately 500 nm of material from the film surface. Following polishing, the sample was meticulously cleaned with an ethanol solution in an ultrasonic cleaner for 3 min. This cleaning steps ensured the removal of any residual SiO_2 suspension particles left from the polishing process. A high-pressure nitrogen blower was then used to dry the sample completely. To investigate the presence of any remaining SiO_2 particles after cleaning, Noran 6 Energy Dispersive X-ray Spectroscopy (EDS) was employed to conduct area mapping of the polished SAC305 film at an accelerating voltage of 15 keV. Finally, the film's crystal structure and orientation were examined using a Bruker-AXS three-circle diffractometer system equipped with a SMART Apex II CCD detector and graphite-monochromated CuK_α radiation. To quantify the surface roughness of the polished films, a Dimension 3100 Digital Instrument Atomic Force Microscope (AFM) from VEECO with a SiO_2 probe tip in tapping mode was utilized.

3 Results and discussion

The process parameters were set at a power of 200 W and a pressure of 0.533 Pa. The deposition was conducted at room temperature. The resulting films exhibited a grain size of 1.65 μm (Fig. 1a). The grain size was determined from the FE-SEM images, and the measurements were analyzed using ImageJ software. However, the film's high roughness posed challenges to obtaining surface measurement due to the AFM tip resolution limitations. The film's structure was notably porous, marked by the distinct grain boundaries, which made nanoindentation tests practically impossible. The substrate temperature was varied to enhance the film's surface morphology; the temperature was increased to 50, and 100 °C while keeping other sputtering parameters constant. At 50 °C, the film's morphology remained unchanged. At 100 °C, the film exhibited disconnected spherical grains with significant grain boundaries, indicating complete melting (Fig. 1b). During the annealing process, it became evident that the films that were exposed to lower temperatures for shorter durations remained unaffected.

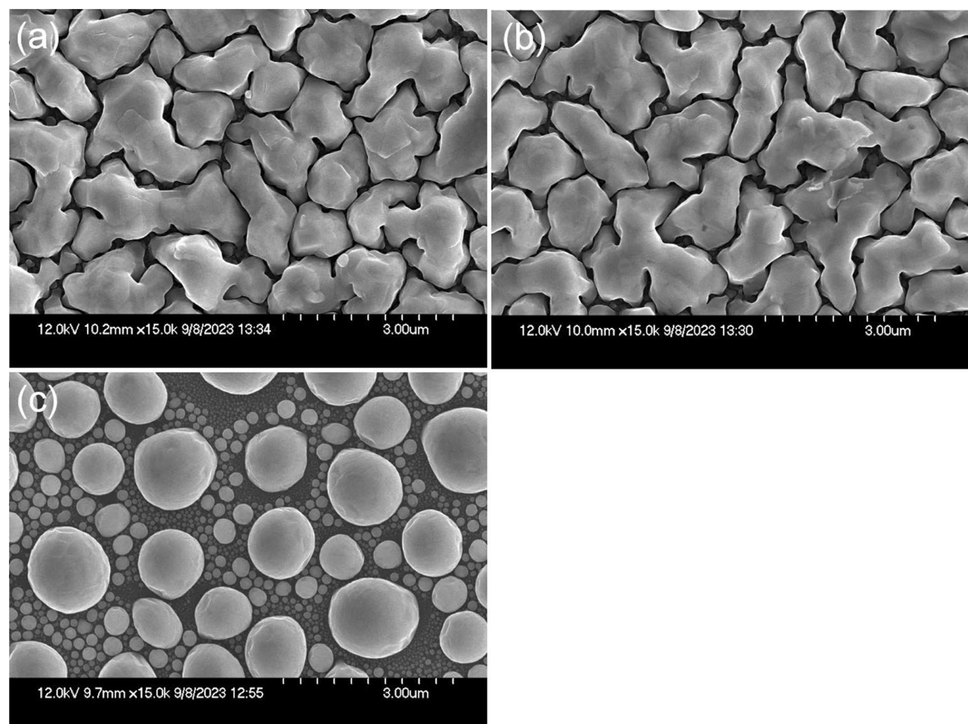

Fig. 1 SAC305 thin film deposition at various temperatures: **a** room temperature, **b** 50 °C, and **c** 100 °C

Also, the film's surface morphology indicated no significant changes when the film was annealed between 120 and 210 °C for 1 to 3 h after deposition. Illustrations of the films that were annealed between 180 and 210 °C are presented in Fig. 2a–f. However, when the annealing conditions were increased to 220 °C for an hour, the films underwent noticeable transformations (Fig. 2g). This transformation included grain growth, the development of voids, and, in some instances, disintegration into separated islands on the substrate. The

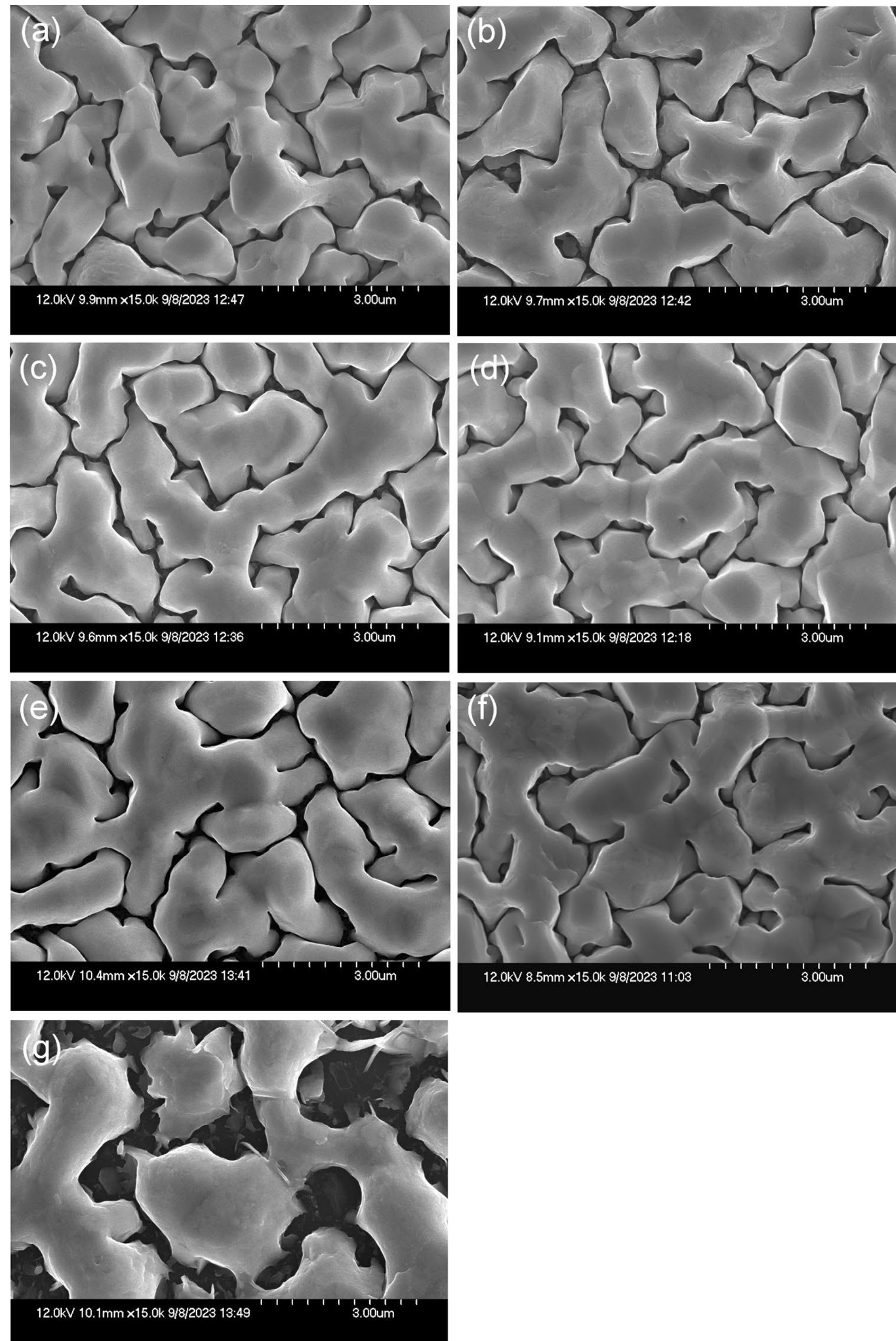

Fig. 2 FE-SEM images of thin SAC305 films after annealing: **a** 180 °C for 1 h, **b** 180 °C for 3 h, **c** 200 °C for 1 h, **d** 200 °C for 3 h, **e** 210 °C for 1 h, **f** 210 °C for 3 h, and **g** 220 °C for 1 h

fabricated SAC305 films' quality was not improved as a result of the above microstructural transformation. These observations were consistent with the findings presented by Abbas et al. (2019) [20]. Based on these results, the emphasis of the study was shifted to the non-annealed films, to explore the influence of varied sputtering parameters on enhancing the surface morphology of the thin films.

In general, DC power is an economical and effective choice for sputtering conductive materials such as metals and transparent conductive oxides. Magnetron DC power sputtering is easy to control because the amount of current and the thickness of the films are almost directly proportional besides the resulting sputtered films exhibit high uniformity [13, 27, 28]. On the contrary, RF magnetron sputtering power is versatile, making it suitable for the deposition of conductive, semiconductive, and insulating materials [13, 27, 28]. The RF power source alternates between positive and negative polarities [13, 27, 28]. During the positive half-cycle, electrons flow to the target surface, neutralizing the accumulated positive charge and enabling positive ions to bombard the target in the negative half-cycle of the RF voltage [13, 27, 28]. The deposition rate is higher for DC compared to RF sputtering and DC sputtering produces high adhesion properties since it requires high energy [13, 27, 28]. SAC305 is a conductive material well-suited for both DC and RF processes.

Figure 3 reveals that the deposition rate increases with increased sputtering power for both DC and RF sputtering processes. This relationship is influenced by the Ar ion flux and its average energy when it collides with the target [29, 30]. Elevated Ar ion flux at higher power typically leads to pronounced ion interactions with the target [29, 30]. Simultaneously, the enhanced kinetic energy of these ions augments the chances of the incident ions dislodging atoms from the target. Both factors, tied to the applied voltage and sputtering power, play pivotal roles in boosting the sputtering deposition rate [29, 30].

The excitation mode notably impacts the deposition rate; for instance, RF sputtering yields a lower deposition rate at an equivalent discharge power than DC sputtering. At lower power levels, specifically at 20 W, the difference in deposition rates between DC and RF sputtering is negligible, amounting to a mere 0.03 Å/s. However, this difference becomes more substantial as the power increases, reaching a difference of 1.05 Å/s at 200 W. This phenomenon can be interpreted as the

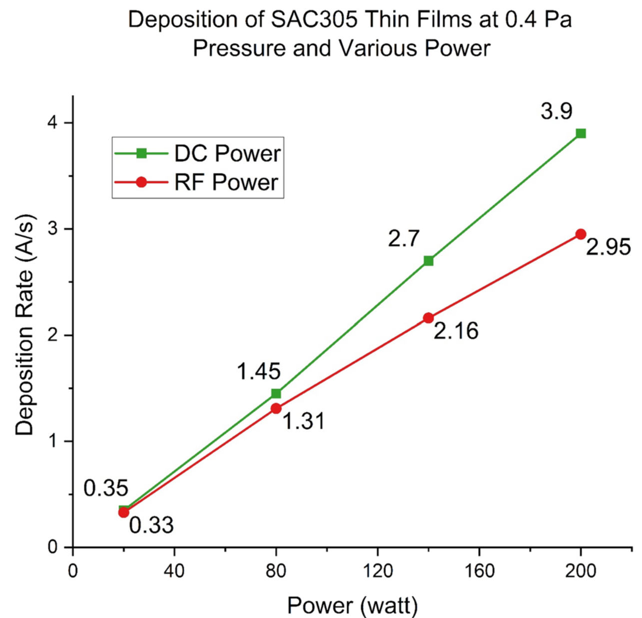

Fig. 3 Variable power effects in magnetron sputtering deposited SAC305 thin films at 0.4 Pa pressure

lower discharge voltage in RF magnetron sputtering exhibits a significantly higher ion flux than the DC magnetron sputtering relative to the neutral particles [27, 28]. If, for example, DC and RF are operating at the same substrate bias voltage and deposition rate, the energy delivered to the fabricated film during RF excitation is considerably more significant than that during DC excitation. However, for the same discharge power, the deposition rate of thin films using a DC magnetron sputtering surpasses that of an RF magnetron sputtering. This difference in the deposition rate can be attributed to the accelerating bias voltage at the cathode in a DC magnetron sputtering, which is particularly higher than in an RF magnetron sputtering [27, 28].

Figure 4 depicts FE-SEM images of the SAC305 films' surface area deposited on Si substrate at powers between 20- and 200-watts using DC and RF sources at various pressures. At a deposition power of 20 W, SAC305 films displayed a fine-grain structure accompanied by larger grain boundaries. The phenomena of smaller grains, combined with voided boundaries, was more profound for RF than DC power. However, when the power was increased to 80 watts, the grain structure for the DC power became denser and the grains were enlarged. A further increase in the DC power supply (140 to 200 watts) did not significantly impact the surface morphology. On the contrary, the

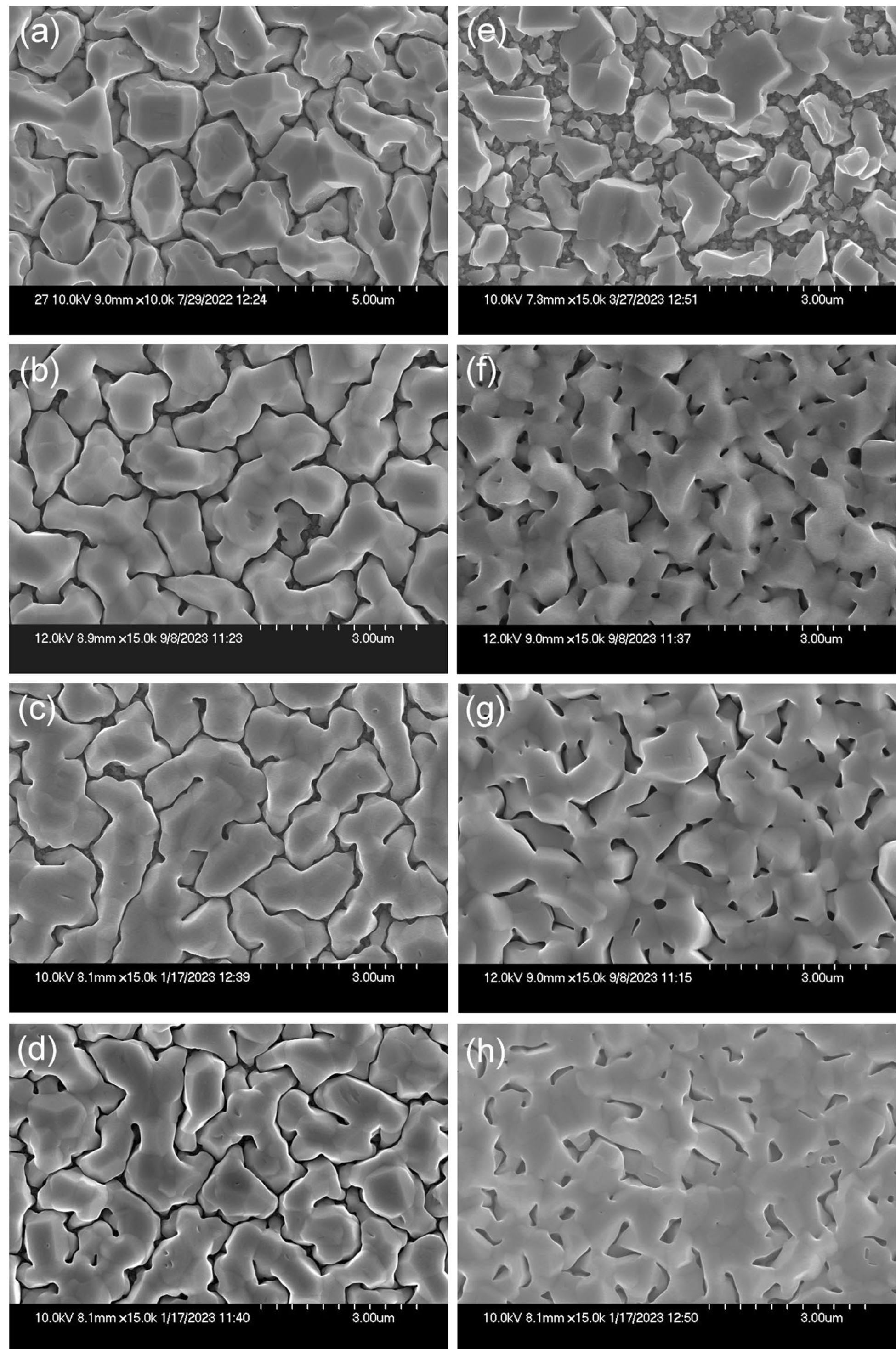

Fig. 4 FE-SEM images of thin SAC305 film surfaces deposited at 0.4 Pa on a Si substrate using various power sources: **a** 20 W DC, **b** 80 W DC, **c** 140 W DC, **d** 200 W DC, **e** 20 W RF, **f** 80 W RF, **g** 140 W RF, and **h** 200 W RF

films that were fabricated using 20 RF power watts depicted a porous structure and they were not continuous in comparison to the films that were fabricated using 80 RF. As the RF power was increased (140 to 200 watts), an obvious improvement was visible in the sample surface morphology, accompanied by an increase in grain size.

The deposition rates of the SAC305 films were investigated for varying deposition pressures ranging from 0.32 to 2.67 Pa at a constant 200-W DC and

RF power supplies. At 0.32 Pa and 200 W power, the deposition rate was 4 Å/s for DC and 3.0 Å/s for RF power supplies, respectively. However, the deposition rate declined as the pressure was increased for both DC and RF power supplies. At 2.67 Pa and 200 W power, the deposition rate was 1.63 Å/s for DC and 1.42 Å/s for RF power supplies, respectively. The observed decrease in deposition rate with increasing deposition pressure can be attributed to collisional events between the sputtered SAC305 atoms and Ar species in the deposition chamber. As the sputtering pressure increases, the collision probability between sputtered and gas particles typically increases, due to the shorter mean free path (MFP) [29, 30]. As a result, some sputtered SAC305 adatoms are deflected away from the substrate, leading to a reduced deposition rate. Figure 5 illustrates the relationship between the deposition rate of SAC305 films and the working pressure for both DC and RF sputtering methods. In both techniques, an increase in the working pressure from 0.32 to 2.67 Pa results in a decline in the deposition rate. The difference in the deposition rates between the two methods is minor at higher pressures, i.e., 0.21 Å/s at 2.67 Pa. However, this gap widens significantly as the pressure decreases, reaching a difference of 1 Å/s at 0.32 Pa. RF sputtering exhibits lower deposition rates at higher pressures which is attributed to an increased atomic scattering. At

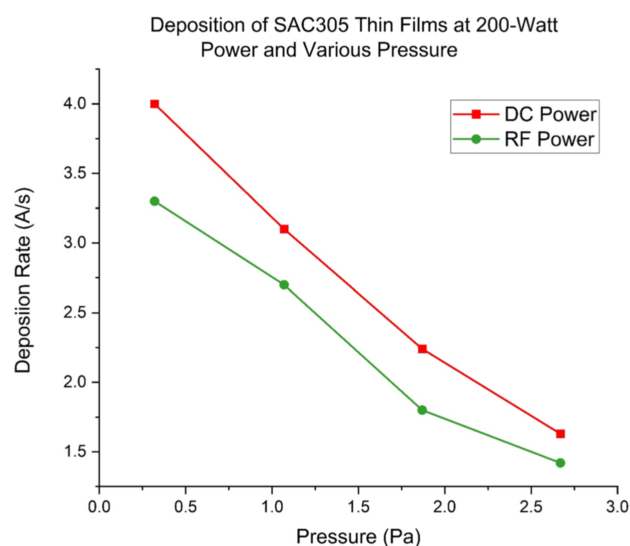

Fig. 5 Variable pressure effects in magnetron sputtering deposited SAC305 thin films at 200-W power

low deposition pressures (0.32 Pa), SAC305 films exhibited a uniform and larger grain structure, Fig. 6. However, as the pressure increased, the grain structure turned into smaller grains accompanied by voided boundaries. At the highest pressure of 2.67 Pa, Fig. 6, more and broader voided boundaries were developed. The increase in sputtering pressure leads to a decrease in the kinetic energy of sputtered adatoms as they undergo a higher number of collisions with Ar gas. This reduced kinetic energy of sputtered adatoms consequently diminishes the surface mobility of the adatoms, hindering their ability to aggregate and grow, resulting in a more porous film microstructure.

In this research, the most favorable SAC305 surface morphology was obtained under low chamber pressure and high power supplied by an RF power source. Specifically, a SAC305 film deposited at a chamber pressure of 0.32 Pa and an RF power of 200 W demonstrated superior surface characteristics compared to other samples before polishing. However, even the best-performing SAC305 sample exhibited a surface that was still too rough for precise AFM measurements. This limitation was attributed to the constraints in the resolution of the AFM tip. The SAC305 films were further deposited on gallium arsenide, sapphire, and glass substrates consistently with the one used above to deposit SAC305 films on Si substrate as previously mentioned at 0.32 Pa and an RF power of 200 watts. Figure 7 shows an FE-SEM image of the SAC305 thin films deposited on (a) silicon, (b) gallium arsenide, (c) sapphire (aluminum oxide), and (d) glass substrates. The SAC305 samples which were deposited on silicon (Si), gallium arsenide (GaAs), and aluminum oxide (Al_2O_3) substrates exhibited porous structures with interconnected nanoparticles. In contrast, the SAC305 sample that was deposited on glass substrates (SiO_2) resulted in distinct nanoparticles with variable sizes and shapes. The porous nature of SAC305 deposited thin films on glass, in comparison to Si substrates, can be explained by the differences in surface properties and interactions. When SAC305 is deposited onto glass surfaces, it tends to form porous structures due to weaker interactions and bonding between the Sn atoms and the glass substrate. In contrast, when SAC305 is deposited onto Si substrates, the presence of a thin interfacial oxide layer promotes stronger chemical bonding between the Sn film and the Si substrate, resulting in a more compact and adherent film with reduced porosity.

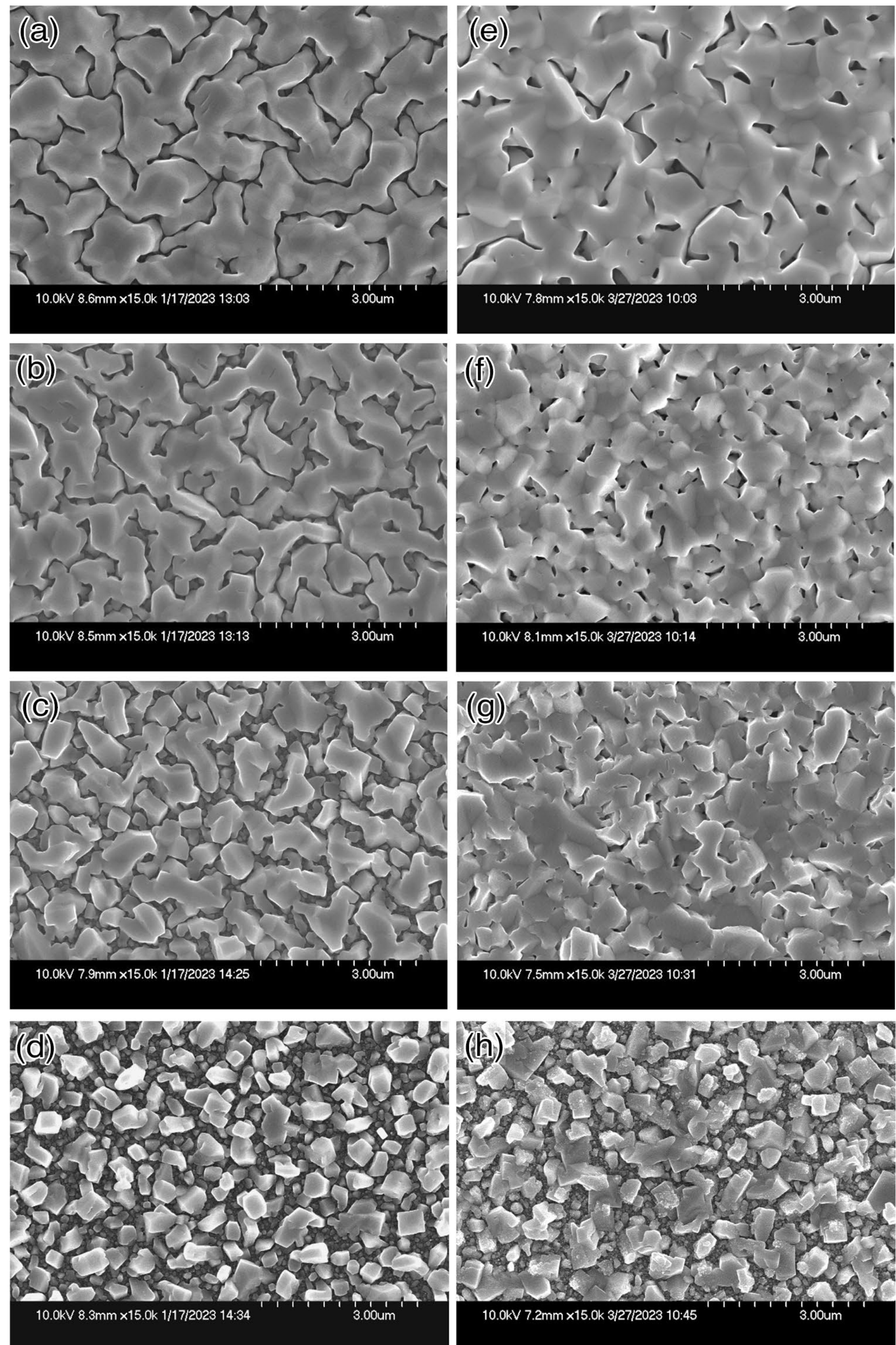

Fig. 6 FE-SEM images of thin SAC305 films deposited on a Si substrate at various pressures using 200 W DC and RF power sources: **a** 0.32 Pa (DC), **b** 1.07 Pa (DC), **c** 1.87 Pa (DC), **d** 2.67 Pa (DC), **e** 0.32 Pa (RF), **f** 1.07 Pa (RF), **g** 1.87 Pa (RF), **h** 2.67 Pa (RF)

XRD diffraction patterns for SAC305 thin film deposited on various substrates are shown in Fig. 8. The samples depicted polycrystalline β-Sn grains, with a preferred diffraction plane of (200) orientation at 2θ of 30.70°. Additionally, weaker peaks of β-Sn were observed at 2θ of 32.09°, 43.97°, 45.00°, 55.46°, 63.93°, 72.59°, and 73.34°, corresponding to diffractions planes of (101), (220), (211), (301), (400), (420), and (411) respectively; however, weaker peaks of Ag_3Sn were observed at 2θ of 37.60° and 39.59°. The peaks

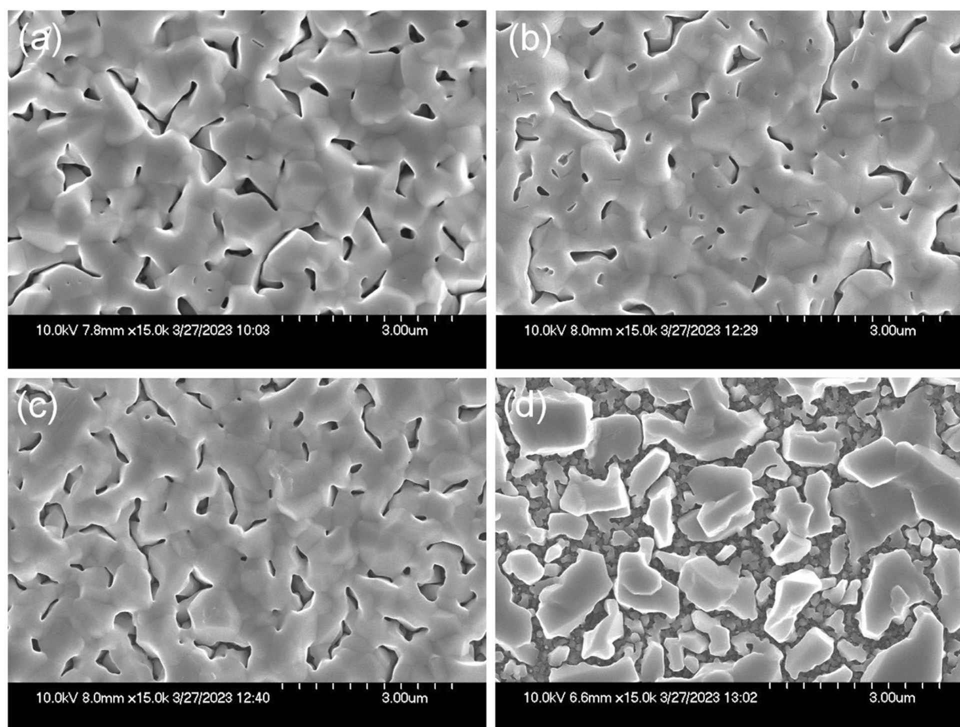

Fig. 7 FE-SEM images of thin SAC305 films deposited at 0.32 Pa using 200 W RF power on various substrates: **a** Si, **b** GaAs, **c** Sapphire, **d** glass

of Ag_3Sn relate to planes (020) and (211), respectively. Since there was no indication of peaks that solely represent Ag, we believe that the Ag adatoms were fully fused with the Sn layer to form an alloy. The Si substrate exhibited a prominent peak at 2θ of 69.15°, corresponding to the (400) plane. In contrast, a weaker peak was observed at 2θ of 33.04° associated with the (200) plane. For GaAs, a peak was detected at 2θ of 31.46° corresponding to the (200) plane. Notably, no peaks corresponding to Al_2O_3 and SiO_2 were observed in the case of sapphire and glass substrates as expected because both are amorphous.

Our focus is still on obtaining continuous robust SAC305 films and we redirected our attention towards polishing the SAC305 thin films to enhance the surface morphology. A SAC305 thin film sputtered on a Si substrate was explicitly selected for this polishing treatment. Sample #13 of Table 2 sputtered with an RF power source at a pressure of 0.32 Pa and a power of 200W on a Si substrate was unequivocally chosen for this polishing treatment as it depicted the most ideal surface morphology among all the other samples.

Since sample 13 of Table 2 represented the best-sputtered sample in terms of the continuity and better surface morphology properties among others, we conducted FE-SEM microscopy analysis of this sample as indicated in Fig. 9. The FE-SEM images in Fig. 9 represent surface morphology and cross-sectional images. Figure 9a and c depict the top surfaces before and after polishing, respectively, while Fig. 9b and d represent the cross-sectional areas before and after polishing, respectively. A polycrystalline structure of grain sizes of 1 μm in diameter was detected before polishing, Fig. 9a. The cross-sectional image of the 2 μm thick film shown in Fig. 9b revealed narrow cones and deep valleys with a peak-to-valley distance of 400 nm. Using a precision automatic polisher, we managed to remove 500 nm of the top surface material of the 2 μm SAC305 thick film in a 2-min polishing period. The SAC305 sample was subsequently cleaned with ethanol in an ultrasonic cleaner for 3 min to remove any SiO_2 suspension particles. The polishing process resulted in a smooth and continuous surface with a uniform thickness of 1700 nm. No traces of Si particles were detected using EDS, indicating that the ultrasonic cleaning process had completely removed the SiO_2 particles. The elemental distribution of Sn, Ag, and Cu are represented by cyan, green, and yellow colors, respectively (Fig. 10).

The surface roughness post-polishing of sample 13 was characterized as represented by the AFM image of Fig. 11. It was not possible to obtain accurate AFM measurements of the surface roughness of the unpolished SAC305 thin film due to the resolution limitation

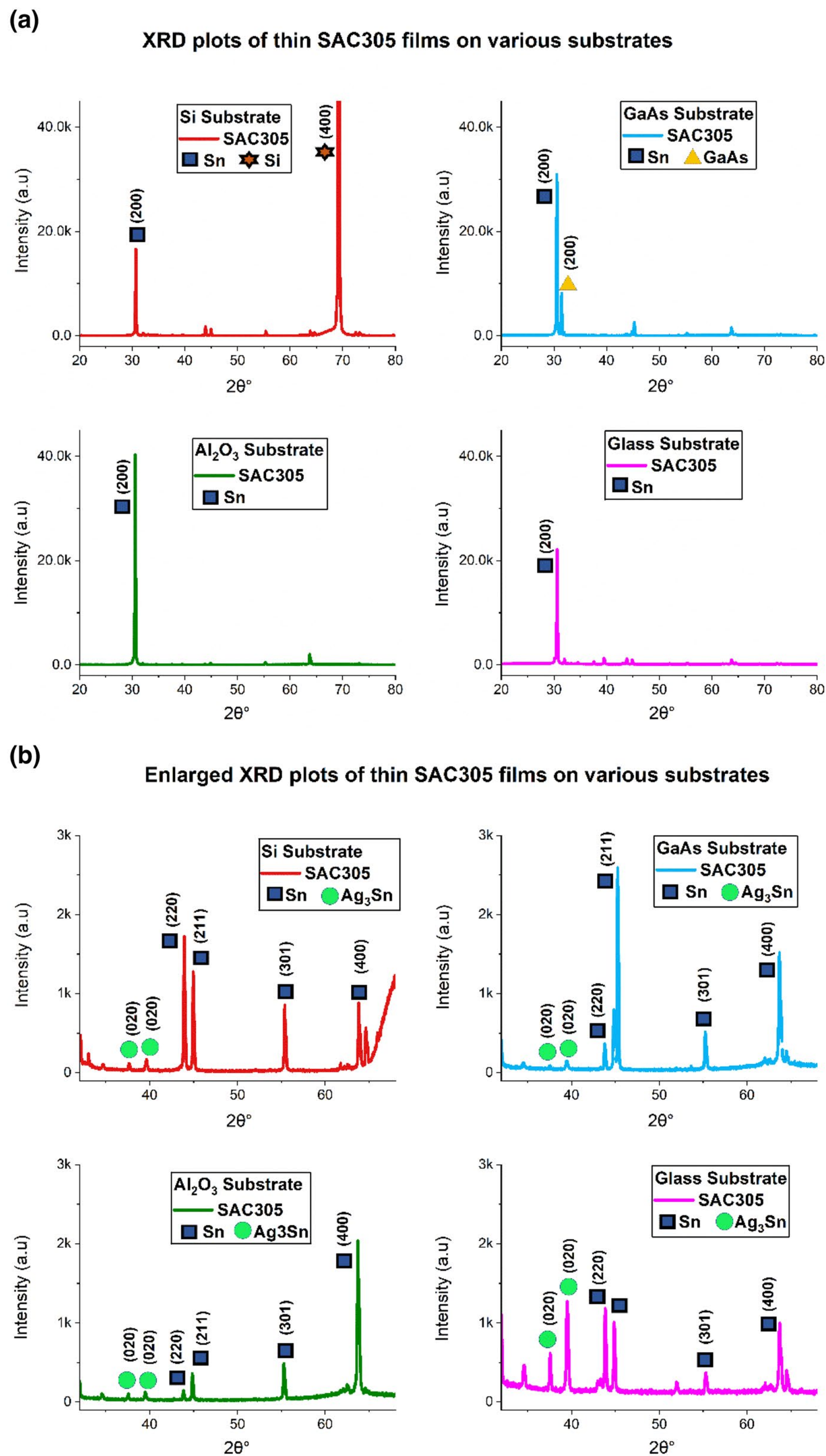

Fig. 8 XRD analysis of thin SAC305 films deposited on various substrates: **a** full XRD patterns. **b** Enlarged view of selected peaks for a closer examination

of the AFM tip. After polishing the SAC305 films which resulted in a film of 1700 nm thickness, an AFM surface measurement was successfully conducted. For the polished SAC305 thin film, the mean roughness (R_a) and root-mean-square roughness (R_q) are 16.9 nm and 24.6 nm, respectively.

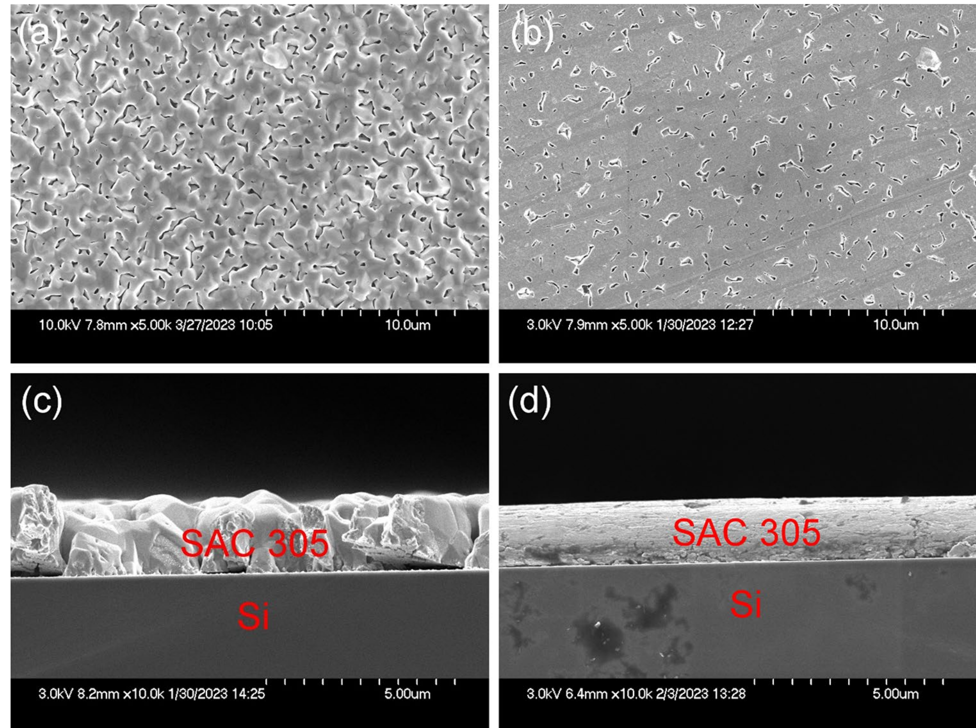

Fig. 9 FE-SEM images of a thin SAC305 film deposited on a Si substrate using 200 W RF power and 0.32 Pa pressure: **a** surface morphology before polishing, **b** surface morphology after 2 min of polishing, **c** cross-sectional morphology before polishing, **d** cross-sectional morphology after 2 min of polishing

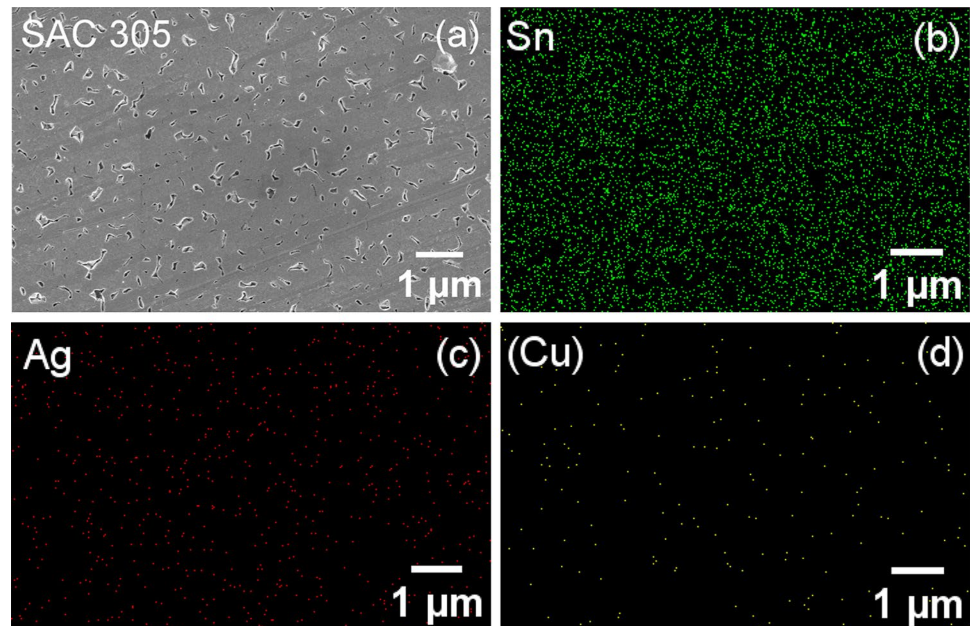

Fig. 10 EDS analysis of the elemental composition of a polished SAC305 thin film after ultrasonic cleaning: **a** elemental map of the surface, **b** distribution of Sn, **c** distribution of Ag, **d** distribution of Cu

4 Conclusion

The results of elevating the substrate temperature beyond 50 °C indicated larger, disconnected, and porous grains, suggesting potential partial melting at 100 °C. It is also noted that annealing effects demonstrated minimal changes up to 210 °C, while significant changes, including grain growth and fragmentation, occurred at an annealing temperature of 220 °C for an hour. The lack of observed morphological changes in the annealed samples likely stems from the relatively low annealing temperature (room

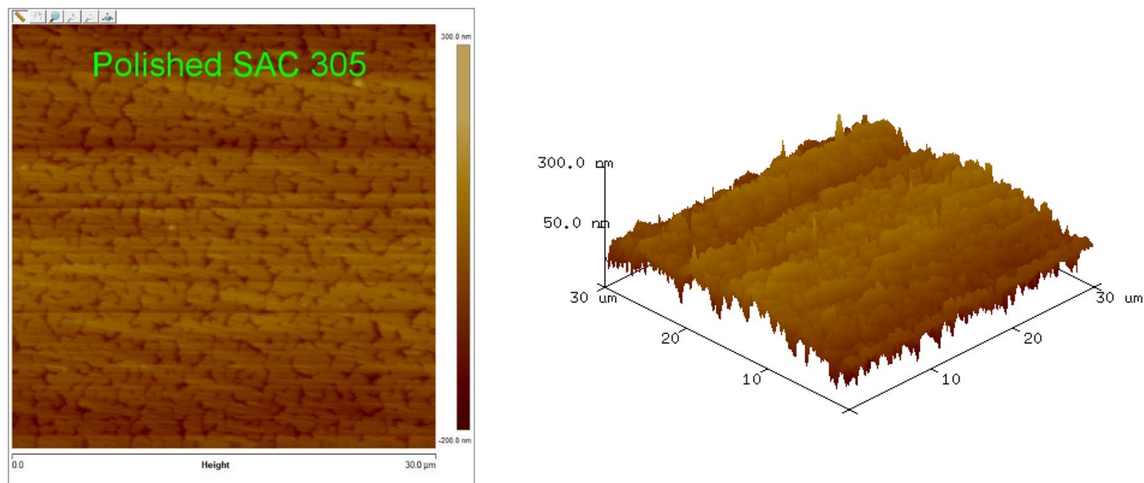

Fig. 11 AFM images (30 μm × 30 μm) of polished SAC305 films on a silicon substrate

temperature) compared to the eutectic temperature of SAC 305 (217 °C). Since solidification occurs at room temperature with minimal heat release, significant temperature-driven modifications to the surface morphology were not observed for annealing temperatures below the eutectic temperature. We conclude that the optimal morphology of the SAC305 films was accomplished using an RF power source of 200 W and 0.32 Pa at room temperature. The analysis of the sputtering parameters including power and pressure indicated that increased sputtering power corresponded to higher deposition rates for both DC and RF techniques, with lower sputtering power levels producing porous films with smaller grain sizes, particularly in SAC305 films produced using RF sputtering power. The deposition rate decreases with increasing the pressure from 0.32 to 2.67 Pa at a sputtering power of 200 watts for both DC and RF sputtering powers. The use of various substrates for deposition indicated morphological variations and XRD diffraction patterns indicated polycrystalline β-Sn grains. The polishing of a selected SAC305 film on a Si substrate resulted in significant improvement in surface roughness.

Acknowledgements

The authors would like to acknowledge the College of William and Mary for the use of the FE-SEM.

Author contributions

All authors contributed to the study conception and design. Material preparation, data collection and analysis were performed by [MO], and [AE]. The first draft of the manuscript was written by [MO] and all authors commented on previous versions of the manuscript. All authors read and approved the final manuscript.

Funding

The authors declare that no funds, grants, or other support were received during the preparation of this manuscript.

Data availability

Data will be available upon request.

Declarations

Conflict of interest The authors declare that they have no known competing financial interests or personal relationships that could have appeared to influence the work reported in this paper.

Open Access This article is licensed under a Creative Commons Attribution 4.0 International License, which permits use, sharing, adaptation, distribution and reproduction in any medium or format, as long as you give appropriate credit to the original author(s) and the source, provide a link to the Creative Commons licence, and indicate if changes were made. The images or other third party material in this article are included in the article's Creative Commons licence, unless indicated otherwise in a credit line to the material. If material is not included in the article's Creative Commons licence and your intended use is not permitted by statutory regulation or exceeds the permitted use, you will need to obtain permission directly from the copyright holder. To view a copy of this licence, visit http://creativecommons.org/licenses/by/4.0/.

References

1. M.B. Kelly, T. Maity, A.R. Nazmus Sakib, D.R. Frear, N. Chawla, Influence of substrate surface finish metallurgy on lead-free solder joint microstructure with implications for board-level reliability. J. Electron. Mater. **49**(5), 3251–3258 (2020). https://doi.org/10.1007/S11664-020-08013-0
2. W. Peng, E. Monlevade, M.E. Marques, Effect of thermal aging on the interfacial structure of SnAgCu solder joints on Cu. Microelectron. Reliab. **47**(12), 2161–2168 (2007). https://doi.org/10.1016/J.MICROREL.2006.12.006
3. K. Suganuma, Advances in lead-free electronics soldering. Curr. Opin. Solid State Mater. Sci. **5**(1), 55–64 (2001). https://doi.org/10.1016/S1359-0286(00)00036-X
4. S.K. Kang, P.A. Lauro, D.Y. Shih, D.W. Henderson, K.J. Puttlitz, Microstructure and mechanical properties of lead-free solders and solder joints used in microelectronic applications. IBM J. Res. Dev. **49**(4–5), 607–620 (2005). https://doi.org/10.1147/rd.494.0607
5. M. Abtew, G. Selvaduray, Lead-free solders in microelectronics. Mater. Sci. Eng. **27**(5–6), 95–141 (2000). https://doi.org/10.1016/S0927-796X(00)00010-3
6. S. Cheng, C.M. Huang, M. Precht, A review of lead-free solders for electronics applications. Microelectron. Reliab. **75**, 77–95 (2017). https://doi.org/10.1016/j.microrel.2017.06.016
7. D.H. Cho, S.M. Seo, J.B. Kim, S.H. Rajendran, J.P. Jung, A review on the fabrication and reliability of three-dimensional integration technologies for microelectronic packaging: through-Si-via and solder bumping process. Metals **11**(10), 1664 (2021). https://doi.org/10.3390/met11101664
8. R.P. Vinci, J.J. Vlassak, Mechanical behavior of thin films. Annu. Rev. Mater. Sci. **26**, 431–462 (1996)
9. R. Schwaiger, O. Kraft, Analyzing the mechanical behavior of thin films using nanoindentation, cantilever microbeam deflection, and finite element modeling. J. Mater. Res. **19**, 31 (2004). https://doi.org/10.1557/jmr.2004.19.1.315
10. D. Beegan, S. Chowdhury, M.T. Laugier, Comparison between nanoindentation and scratch test hardness (scratch hardness) values of copper thin films on oxidized silicon substrates. Surf. Coat. Technol. **201**(12), 5804–5808 (2007). https://doi.org/10.1016/J.SURFCOAT.2006.10.031
11. A. Baptista, F. Silva, J. Porteiro, J. Míguez, G. Pinto, Sputtering physical vapor deposition (PVD) coatings: a critical review on process improvement and market trend demands. Coatings **8**(11), 402 (2018). https://doi.org/10.3390/coatings8110402
12. S. Hogmark, S. Jacobson, M. Larsson, Design and evaluation of tribological coatings. Wear **246**(1–2), 20–33 (2000). https://doi.org/10.1016/S0043-1648(00)00505-6
13. P.J. Kelly, R.D. Arnell, Magnetron sputtering: a review of recent developments and applications. Vacuum **56**(3), 159–172 (2000). https://doi.org/10.1016/S0042-207X(99)00189-X
14. L.M. Lee, A.A. Mohamad, Interfacial reaction of Sn-Ag-Cu lead-free solder alloy on Cu: a review. Adv. Mater. Sci. Eng. **2013**, 11 (2013). https://doi.org/10.1155/2013/123697
15. K.S. Kim, S.H. Huh, K. Suganuma, Effects of Intermetallic Compounds on Properties of Sn–Ag–Cu Lead-Free Soldered Joints. J. Alloy Compd. **352**(1–2), 226–236 (2003). https://doi.org/10.1016/S0925-8388(02)01166-0
16. K.Y. Chan, B.S. Teo, Sputtering power and deposition pressure effects on the electrical and structural properties of copper thin films. J. Mater. Sci. **40**, 5971–5981 (2005). https://doi.org/10.1007/s10853-005-1362-8
17. H.N. Shah, R. Jayaganthan, D. Kaur, Effect of sputtering pressure and temperature on DC magnetron sputtered CrN films. Surf. Eng. **26**(8), 629–637 (2010). https://doi.org/10.1179/174329409X389326
18. L.B. Freund, S. Suresh, *Thin Film Materials: Stress, Defect Formation, and Surface Evolution* (Cambridge University Press, Cambridge, 2004)
19. A. González-González, G.M. Alonzo-Medina, A.I. Oliva, C. Polop, J.L. Sacedón, E. Vasco, Morphology evolution of thermally annealed polycrystalline thin films. Phys. Rev. B **84**(15), 155450 (2011). https://doi.org/10.1103/PhysRevB.84.155450
20. N. Abbas, M.R. Shad, M. Hussain, S.M.Z. Mehdi, U. Sajjad, Fabrication and characterization of silver thin films using physical vapor deposition, and the investigation of annealing effects on their structures. Mater. Res. Express

6(11), 116437 (2019). https://doi.org/10.1088/2053-1591/ab4c4f

21. W.J. Liu, Y.H. Chang, C.C. Chiang, Y.T. Chen, Y.Z. Wang, C.L. Wu, S.L. Ou, Thickness, annealing, and surface roughness effect on magnetic and significant properties of $Co_{40}Fe_{40}B_{10}Dy_{10}$ thin films. Materials **16**(17), 5995 (2023). https://doi.org/10.3390/ma16175995
22. I.C. Sburlan, I. Vasile, E. Tudor, Comparative study between semiconductor power devices based on silicon (Si), silicon carbide (SiC), and gallium nitrate (GaN) used in the electrical system subassembly of an electric vehicle. International Semiconductor Conference, Romania, 107–110. IEEE (2021). https://doi.org/10.1109/CAS52836.2021.9604127.
23. A. Tanaka, Toxicity of indium arsenide, gallium arsenide, and aluminum gallium arsenide. Toxicol. Appl. Pharmacol. **198**(3), 405–411 (2004). https://doi.org/10.1016/j.taap.2003.10.019
24. M.S. Akselrod, F.J. Bruni, Modern trends in crystal growth and new applications of sapphire. J. Cryst. Growth **360**, 134–145 (2012). https://doi.org/10.1016/j.jcrysgro.2011.12.038
25. M. Ojha, Y. Mohammed, D.S. Stone, A.A. Elmustafa, Microstructure, creep properties, and electrical resistivity of magnetron sputtering deposited SAC305 thin films. J. Vac. Sci. Technol. B **41**(5), 2205 (2023). https://doi.org/10.1116/6.0002949
26. W. Kern, The evolution of silicon wafer cleaning technology. J. Electrochem. Soc. **137**(6), 1887 (1990). https://doi.org/10.1149/1.2086825
27. Z. Li, W. Gao, ZnO thin films with DC and RF reactive sputtering. Mater. Lett. **58**(7–8), 1363–1370 (2004). https://doi.org/10.1016/j.matlet.2003.09.028
28. S. Tan, X. Zhang, X. Wu, F. Fang, J. Jiang, Comparison of chromium nitride coatings deposited by DC and RF magnetron sputtering. Thin Solid Films **519**(7), 2116–2120 (2011). https://doi.org/10.1016/j.tsf.2010.10.067
29. J. Bohlmark, M. Lattemann, J.T. Gudmundsson, A.P. Ehiasarian, Y. Aranda Gonzalvo, N. Brenning, U. Helmersson, The ion energy distributions and ion flux composition from a high-power impulse magnetron sputtering discharge. Thin Solid Films **515**(4), 1522–1526 (2006). https://doi.org/10.1016/J.TSF.2006.04.051
30. E. Kusano, K. Fukushima, T. Saitoh, S. Saiki, N. Kikuchi, H. Nanto, A. Kinbara, Effects of Ar pressure on ion flux energy distribution and ion fraction in R.F.-plasma-assisted magnetron sputtering. Surf. Coat. Technol. **120**, 189–193 (1999). https://doi.org/10.1016/S0257-8972(99)00453-3

Publisher's Note Springer Nature remains neutral with regard to jurisdictional claims in published maps and institutional affiliations.